Comparison of water surface temperature retrieval methods from Landsat 9 satellite data

Matias Bonansea [1,2], Sofia Gutierrez [1], Mariana Correa [1], Sofia Pana [3], Victor Gauto [3], Francisco Nemiña [3], Alba Germán [3], Giuliana Beltramone [3], Lucio Pinotti [1,2], Anabella Ferral [3]

[1] Instituto de Ciencias de la Tierra, Biodiversidad y Ambiente (ICBIA, CONICET-UNRC) – Ruta 36, Km 601, Río Cuarto, Córdoba, Argentina – (mbonansea, sgutierrez)@exa.unrc.edu.ar

[2] Departamento Geología, Facultad de Ciencias Exactas Físico-Químicas y Naturales, Universidad Nacional de Río Cuarto (UNRC), Argentina

[3] Instituto de Altos Estudios Espaciales Mario Gulich, Centro Espacial Teófilo Tabanera, CONAE, Argentina

Keywords: Landsat Collection 2 Level 2 products, Single-Channel method, Split-Window algorithm, Surface temperature.

Abstract

Water surface temperature (WST) is a crucial parameter in aquatic systems, influencing both water quality and hydrodynamic conditions of these systems. Landsat 9, the latest satellite in the Landsat program, offers a unique opportunity for retrieving Earth's surface temperature data. Despite numerous efforts to develop methods for retrieving surface temperature from remote sensing data, there have been relatively few studies comparing the performance of these methods. The main objective of this study was to evaluate and compare the effectiveness of various methods for estimating WST in a reservoir on Argentina using thermal images from the new Landsat 9 satellite. WST retrievals were obtained from Landsat Collection 2 (C2), Level 2 products, as well as from the Single-Channel (SC) method and a Split-Window (SW) algorithm applied to Landsat C2, Level 1 images. The comparative analysis showed that, although all three methods performed similarly, the Split-Window method proved to be the most effective for estimating WST in the Río Tercero reservoir (R^2 = 0.99, RMSE = 0.77 °C). Finally, this method was used to produce detailed WST distribution maps for the studied reservoir

1. Introduction

Water surface temperature (WST) is one of the key parameters in many physical, chemical, and biological processes of aquatic systems, affecting water quality and hydrodynamic conditions of these systems. Furthermore, accurate global measurements of WST are critical to our understanding of global warming and climate change (GCOS, 2016; Fuso et al., 2023).

Conventional methods to measure water temperature are based on in-situ measurements. However, these methods are point character, have logistic limitations, are costly and time consuming, and are often not representative for complex and dynamic ecosystems such as lakes and reservoirs (Dyda et al., 2022; Bonansea et al., 2021). On the other hand, satellite remote sensing is a cost-effective powerful tool to assess water quality and WST at regional and global scales (Meng et al., 2019).

Retrieving surface temperature from space is currently possible by various remote sensing platforms (Jungkeit-Milla et al., 2024). The Landsat Program provides a particular opportunity for the surface temperature retrieval, as it has an uninterruptedly long data record period, since Landsat 3 satellite was launched in 1978 (Markham et al., 2004). The latest satellite of the Landsat program, Landsat 9, was launched on September 27, 2021, and it is operational since February 2022. This new satellite increases as never before the number of Landsat-like satellites in orbit, representing a great potential for data availability and suitability for several applications (Wulder et al., 2022;).

Nowadays, Landsat 9, together with Landsat 8, provide a full coverage of the Earth's surface every 8 days. The Landsat 9 is equipped with the Thermal Infrared Sensor 2 (TIRS-2), and like the TIRS-1 in Landsat 8, this instrument has two thermal-infrared (TIR) bands, that can provide valuable surface temperature records at high spatial resolution since most of the energy detected by the sensor is directly emitted by the land surface (Yu et al., 2014; Niclòs et al., 2023).

Many efforts have been developed to generate retrieval methods of surface temperature from remote sensing data (Gerace et al., 2020). However, few studies have been carried out to compare the performance of these methods (Vanhellemont et al., 2020). In addition, different authors suggest that suitable validation activities based on independent ground-data are required to evaluate the accuracy of different methods used to estimate surface temperature by remote sensing data (Tavares et al., 2019; Niclòs et al., 2023). Therefore, the main objective of this study is to evaluate and compare the effectiveness of different methods to estimate SWT in a reservoir of Argentina based on thermal images from the newest Landsat 9 satellite. The structure of this study is organized as follows. We have described the methodology used in the field, the satellite data and the different methods used to estimate WST in Section 2. The results and analysis are presented in Section 3. Finally, the conclusions are presented in Section 4.

2. Methods

2.1 Study area and field campaigns

The Río Tercero reservoir is located in the province of Córdoba (Argentina) (Figure 1). This reservoir has an area of 46 km^2, a volume of 10 hm^3, a maximum and mean depth of 46.5 and 12.2 m respectively. The Río Tercero reservoir has multiple purposes, such as water supply, power generation, flood control, irrigation,

tourism and recreational activities (Bonansea et al., 2021). In 1986, a nuclear power plant was installed in its south shore. Water for cooling the nuclear reactor is taken from the middle section of the reservoir and is returned to the western basin by a 5 km long open-sky channel (Figure 1). The discharge of warm water from the nuclear power plant creates a thermal plume in the waters of the reservoir, making it an ideal location to evaluate the effectiveness of different methods for retrieve WST by remote sensing.

As part of various water quality monitoring programs, the Río Tercero reservoir has been assessed since 2010. For this study, sampling campaigns that were carried out on August 23, 2022, and December 13, 2022, at eleven sampling sites were evaluated (Figure 1). Coordinates of sampling sites were recorded using a hand-held GPS device. In-situ measurements of WST where conducted using a thermometer at 0.2 m depth.

2.2 Satellite data

Landsat 9, which is a partnership between NASA and the U.S. Geological Survey, continues the Landsat Program's critical role in monitoring, understanding and managing the land resources needed to sustain human life. This satellite carries two sensors, the Operational Land Imager (OLI) and the TIR sensor. The OLI instrument is a 9-band multispectral instrument that covers the visible (VIS), near infrared (NIR), and short-wave infrared (SWIR) regions of the spectrum at 30 m spatial resolution in 8 channels, and at 15 m resolution in the panchromatic channel (Wulder et al., 2022). Information of Landsat 9 satellite resolutions is shown in Table 1. The TIR sensor has two channels in the thermal infrared region with wavelengths centred on 10.9 µm (Band 10: 10.6-11.2 µm) and 12.0 µm (Band 11: 11.5-12.5 µm). The spatial resolution of thermal bands is 100 m, however is resampled by cubic convolution to 30 m matching the OLI grid (Irons et al., 2012). Detailed information about the Landsat 9 satellite can be found on page https://www.usgs.gov/landsat-missions/landsat-9.

In conjunction with fieldwork activities, free-cloud Landsat 9 images of the studied area (Path 229, Row 82), acquired on August 23, 2022, and December 13, 2022, were downloaded from the US Geological Survey (USGS) Earth Explorer website (https://www.usgs.gov/). These images were downloaded as Collection 2 (C2), Level 1 (L1), and Level 2 (L2) products.

Collection 2 processing, which is available since January 1, 2022, contains several enhancements compared to Collection 1 (C1), including several radiometric calibration improvements and new relative gains to reduce along track string that progressively got worse during the mission (NASA, 2024). This collection includes Landsat L1 and L2 data. Landsat C2-L1 data products consist of radiometrically calibrated and geometrically corrected Digital Numbers (DNs) which represent the multispectral image data (NASA, 2024). Landsat C2-L2 data, which are generated from C2-L1 imagery, contains surface reflectance and surface temperature science products. The surface temperature product is generated from the Single-Channel algorithm version 1.3.0 applied to the C2-L1 TIRS band 10 (NASA, 2024). Further information about the applied technique is widely discussed by Malakar et al. (2018).

Once image pre-processing was complete, an unsupervised classification analysis based on ISODATA clustering was performed on each image to mask out terrestrial features (Olmanson et al., 2016) creating images that only contain the Río Tercero reservoir.

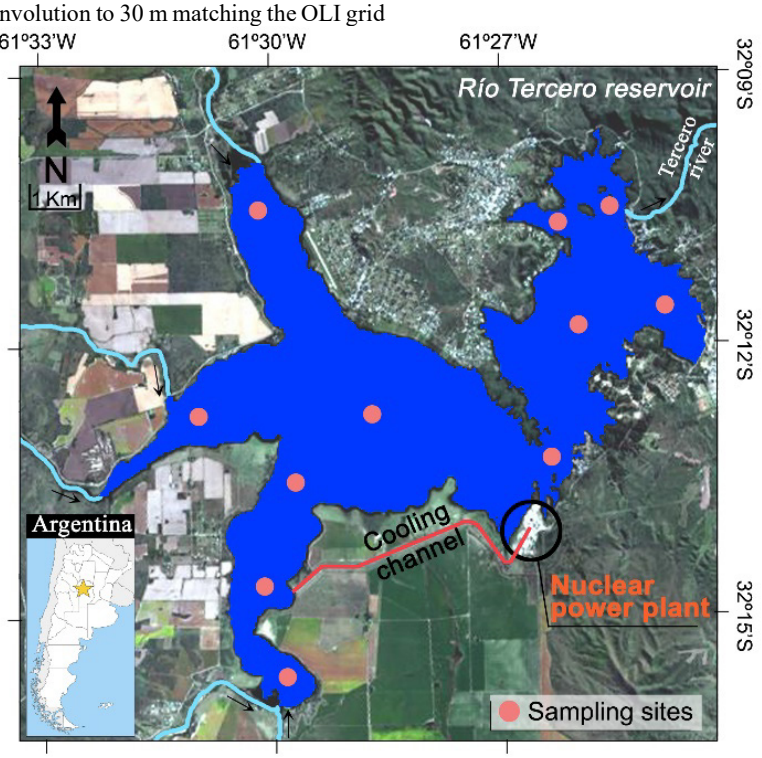

Figure 1. Study area and location of sampling sites.

Band number	Description	Wavelength (µm)	Spatial resolution (m)
1	Coastal / Aerosol	0.43 – 0.45	30
2	Visible blue	0.45 – 0.51	30
3	Visible green	0.53 – 0.59	30
4	Visible red	0.63 – 0.67	30
5	Near-infrared	0.85 – 0.87	30
6	Short infrared	1.56 – 1.65	30
7	Short infrared	2.10 – 2.29	30
8	Panchromatic	0.50 – 0.67	15
9	Cirrus	1.36 – 1.38	30
10	Thermal infrared 1	10.60 – 11.19	100
11	Thermal infrared	11.50 – 12.51	100
Radiometric resolution: 14 bits. Temporal resolution: 16 days.			

Table 1. Band specifications for thermal bands of Landsat 9 sensor.

2.3 Methods used to estimate surface temperature

To compare different methods for estimating WST, we used WST data obtained from Landsat C2-L2 products and also we have applied the Single-Channel (SC) method and a Split-Window (SW) algorithm to Landsat C2-L1 images. These approaches were utilized to retrieve the WST for the Río Tercero reservoir.

2.3.1 Landsat 2 Collection 2: To estimate WST in degrees Celsius (°C) from Landsat C2-L2 products, the equation 1 was used (Crawford et al., 2023):

$$\mathrm{WST} = DN * 0.00341802 + 149 - 273.15 \quad (1)$$

2.3.2 Single-Channel: On the other hand, DNs of Landsat 9 TIRS C2-L1 data were first converted to at-sensor spectral radiance (L_λ) using the equation 2:

$$L_\lambda = gain * DN + bias \quad (2)$$

where *gain, bias* = calibration parameters provided in metadata file of each Landsat scene and presented in Table 2.

L_λ values were, then, converted to at-sensor radiative temperature (Tsen) using the following equation based on Planck's law (adapted for Landsat, specifically) (Chandler et al., 2009):

$$T_{sen} = \frac{k_2}{ln\left(\frac{k_1}{L_\lambda}+1\right)} \quad (3)$$

where k_1, k_2 = thermal conversion constants obtained from the metadata file (Table 2).

Band	Gain	Bias	K_1 ($Wm^{-2}sr^{-1}*\mu m$)	K_2 (K)	Water emissivity (ε)
10	0.00038	0.1	799.03	1329.24	0.992
11	0.00035	0.1	475.6581	1198.35	0.998

Table 2. Band specifications for thermal bands of Landsat 9 sensor

According to different authors, the SC method is a widely used algorithm for surface temperature due to its simplicity and robustness (Bonansea et al., 2019). The SC algorithm uses a single thermal band (Band 10 for Landsat satellites). In this study, a general SC method proposed by Jimenez-Muñoz et al. (2014) was used. The equation for this SC method is shown in equation 4:

$$WST = \gamma[\varepsilon^{-1}(\psi_1 L_\lambda + \psi_2) + \psi_3] + \delta \quad (4)$$

where γ, δ = parameters dependent on the Planck's function (equation 5 and 6) , respectively

ε = water emissivity

ψ_1, ψ_2, ψ_3 = atmospheric functions which were calculated by a MODTRAN simulation procedure (equation 7) (Jimenez-Muñoz et al., 2014)

$$\gamma = \left\{\frac{c_2 L_\lambda}{T_{sen}^2}\left[\frac{\lambda_{ef}^4}{c_1}L_\lambda + \lambda_{ef}^{-1}\right]\right\}^{-1} \quad (5)$$

where c_1, c_2 = Planck's radiation constants (c_1= 1.19104x10^8, c_2= 14387.7) (Jimenez-Muñoz et al., 2014)

λ_{ef} = effective band wavelength which is 10.896 µm for band 10

$$\delta = -\gamma L_\lambda + T_{sen} \quad (6)$$

$$\begin{bmatrix}\psi_1\\ \psi_2\\ \psi_3\end{bmatrix} = \begin{bmatrix}0.04019 & 0.02916 & 1.01523\\ -0.38333 & -1.50294 & 0.20324\\ 0.00918 & 1.36072 & -0.27514\end{bmatrix}\begin{bmatrix}w^2\\ w\\ 1\end{bmatrix} \quad (7)$$

where w = water vapour content (gr/cm^2) obtained from the University of Wyoming online database (http://weather.uwyo.edu/upperair/sounding.html) and coefficients are estimated by simulation. More details about the derivation of this method can be found in Jiménez-Muñoz et al. (2014).

2.3.3 Split-Window: As TIRS-2 has two spectrally adjacent thermal bands, it is suitable to apply a SW algorithm. The basis of the SW algorithm is that the radiance attenuation for atmospheric absorption is proportional to the radiance difference of simultaneous measurements at two different wavelengths, each subject to different amounts of atmospheric absorption (Jimenez-Muñoz et al., 2014). In this study, the SW improved by Gerace et al. (2020) for Landsat 8 and 9 was applied according to equation 8:

$$WST = b_0 + \left(b_1 + b_2\frac{1-\epsilon}{\epsilon} + \frac{\Delta\epsilon}{\epsilon^2}\right)\frac{T_{sen\_i} + T_{sen\_j}}{2} + \left(b_4 + b_5\frac{1-\epsilon}{\epsilon} + b_6\frac{\Delta\epsilon}{\epsilon^2}\right)\frac{T_{sen\_i} - T_{sen\_j}}{2} + b_7\left(T_{sen\_i} - T_{sen\_j}\right)^2 \quad (8)$$

where bk (k= 0 to 7) = sensor-dependent coefficients (Gerace et al., 2020)

i, j = correspond to the Bands 10 and 11 for TIR-2.

ε = average of the band-effective emissivities

Δε = difference in band-effective emissivities (Table 2)

2.4 Methods validation

To assess the accuracy of the used methods, estimated WST values by the different methods were compared to WST values measured in the Río Tercero reservoir during sampling campaigns by simple regression analysis. The coefficient of Pearson correlation (R^2) and the root mean square error (RMSE) between measured and predicted WST values were also used for validation.

Finally, the model with the greatest R^2 and the lowest RMSE was selected to represent the spatial distribution of WST in the Río Tercero reservoir.

3. Results

Table 3 summarizes the basic statistics of WST measurements taken in the Río Tercero reservoir during the sampling campaigns. As expected, the measurements from December recorded higher water temperatures compared to those from August, which can be attributed to the relationship between water temperature and ambient atmospheric conditions. When analyzing the spatial variability of the WST, it was observed that on both sampling dates, WST values were higher near the outlet of the nuclear power plant's cooling channel.

Sampling date	Mean ± Sd. (°C)	Range (Min-Max) (°C)
August 23, 2022	14.3±2.5	11.8-18.4
December 13, 2022	27.2±0.8	26.0-28.6

Table 3. Basic statistics of WST measured in Río Tercero reservoir. Sd.: Standard deviation

Observed values were compared with retrieved WST data obtained by different methods. Figure 2 illustrates the comparison between field measurements and WST values estimated by Landsat 9 satellite. This figure demonstrates that all three methods yielded a strong fit in the regression analysis, indicating a high level of agreement between the gradient and intercept of the regression lines.

Analyzing the results, the SW method improved by Gerace et al. (2020) yielded the most accurate temperature predictions. However, the differences between this method and the others were minimal. Goodness-of-fit measures for the SW method were R2= 0.99 and RMSE= 0.77 °C.

Finally, spatial distribution maps of WST in the Río Tercero reservoir were retrieved using Landsat 9 satellite data (Figure 3). Using the SW algorithm, it was possible to predict the WST across the entire surface of the reservoir, allowing for the correct assessment of the spatial distribution of this variable. Consistent with the sampling campaigns, Figure 3 shows that the highest and most uniform WST values were recorded on December 13, 2022.

Analyzing the spatial distribution, higher WST values were observed near the outlet of the nuclear power plant’s cooling channel, while the lowest values were found in the eastern region of the reservoir. Using satellite data, a thermal plume signature associated with higher WST values and related with the cooling channel of the nuclear power plant, can be identified. On August 23, 2022, this plume was particularly evident, appearing as a broad line of dissipation that is widest near the cooling channel and gradually extends throughout the rest of the reservoir.

Water temperature is one of the most important factors to control the functioning of aquatic systems (Ding and Elmore, 2015). In previous research studies, using Landsat 7 and 8 data, we have assessed the effect of the warm water discharge of the nuclear power plant on the water temperature of the Río Tercero reservoir (Bonansea et al., 2021). Further, we have evaluated the benefits of using a Landsat derived-WST dataset to estimate the probability of Saprolegniasis in this reservoir (Bonansea et al., 2019), which is one of the most economical and ecologically harmful diseases in different species of fish worldwide (Singh et al., 2018).

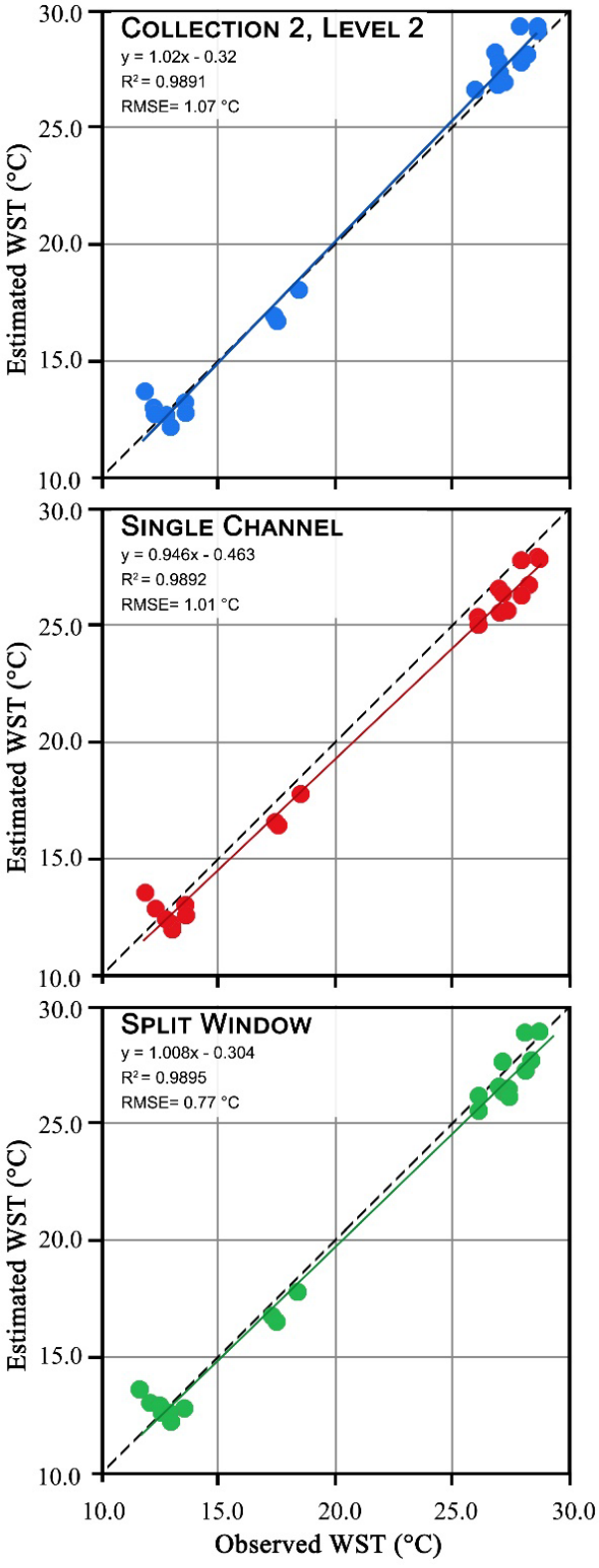

Figure 2. Plots of observed versus estimated WST in Río Tercero reservoir with 1:1 fit line.

In the present study, we have expanded the operational applications of the Landsat Program to enhance the understanding of WST estimation methods in a reservoir of Argentina, using thermal imagery from the latest Landsat 9 satellite. These findings provide a different approach for the

estimation and mapping of water temperature, since water quality assessment in developing countries remains largely unexplored.

Monitoring WST offers significant economic and social benefits. Economically, it enhances water resource management, supports fisheries, optimizes power generation, and boosts tourism by maintaining ideal water conditions. Socially, WST monitoring protects public health by detecting harmful algal blooms, aids in climate change adaptation, and supports environmental conservation by protecting aquatic ecosystems. Overall, it contributes to efficient resource use, public safety, and long-term sustainability.

4. Conclusion

Satellite imagery is a crucial tool for monitoring water quality. This study is among the first to demonstrate the effectiveness of the newest Landsat 9 satellite for retrieving WST data in an aquatic system. The effectiveness of three methods for estimating water temperature was compared.

The comparative analysis reveals that, while all three methods performed similarly, the Split-Windows method developed by Gerace et al. (2020) was the most effective for estimating WST in the Río Tercero reservoir. Although the SW method is the best for estimating water temperature, due to its rapid and easy implementation, Landsat C2-L2 data products can also be highly recommended for observing Earth's surface temperature.

Furthermore, detailed WST distribution maps were obtained, and the thermal plume generated by the nuclear power plant was clearly detectable. This thermal plume generates a dissipation line that is widest near the cooling channel and gradually extends throughout the rest of the reservoir. This study offers a novel method for estimating and mapping water temperature, providing valuable information for environmental managers.

Acknowledgements

This research study was financially supported by the CONICET, FONCyT, grant number [PICT-2021-GRF-TII-00393]. The authors would like to thank to the Dirección de Seguridad Náutica (DSN) and Departamento de Unidades de Alto Riesgo (DUAR) of Córdoba province for their collaboration in sampling campaigns. The reviewers and the editor are thanked for their insightful comments which helped to improve this paper.

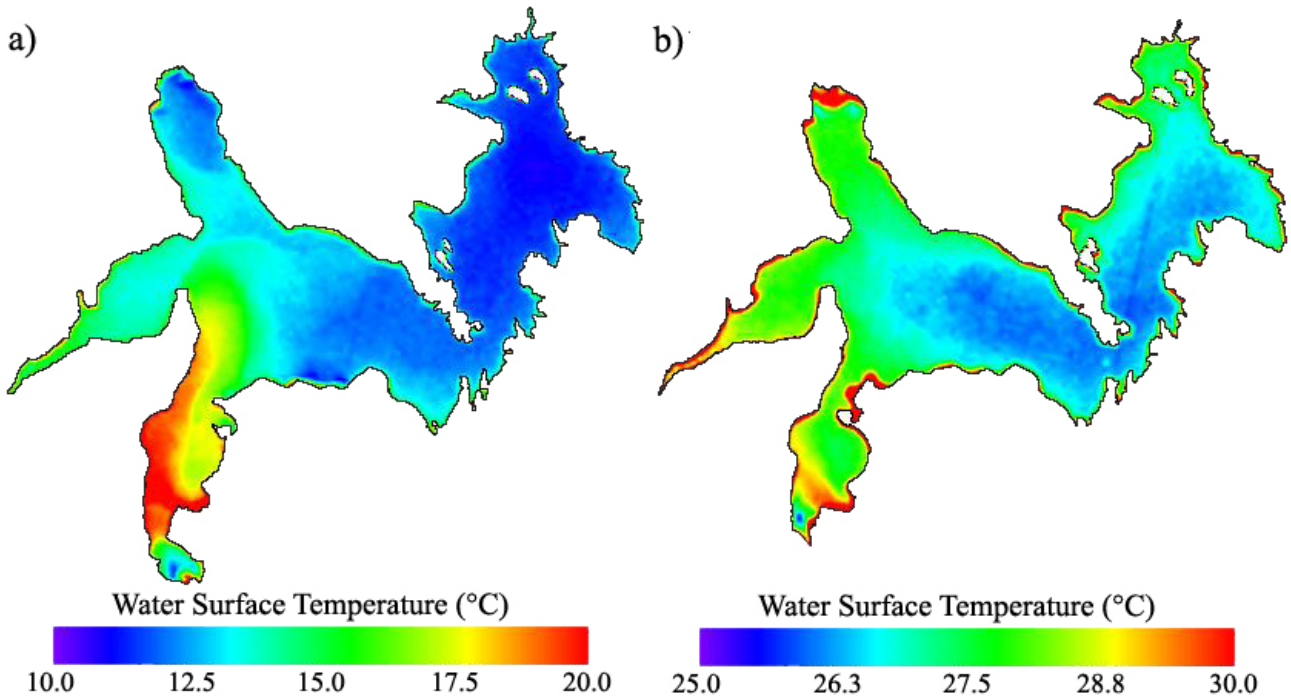

Figure 3. Water surface temperature for the Río Tercero reservoir using Landsat 9 images.
a) August 23, 2022.b) December 13, 2022

References

- Bonansea, M., Mancini, M., Ledesma, M., Ferrero, S., Rodriguez, C., Pinotti. L., 2019, Remote sensing application to estimate fish kills by Saprolegniasis in a reservoir. *Science of the total Environment*, 669: 930-937. doi.org/10.1016/j.scitotenv.2019.02.442.

Bonansea, M., Ferrero, S., Ferral, A., Ledesma, M., German, A., Carreño, J., Pinotti, L., 2021: Assessing water surface temperature from Landsat imagery and its relationship with a nuclear power plant. *Hydrological Sciences Journal*, 66(1), 50-58. doi.org/10.1080/02626667.2020.1845342.

Chandler, G., Markham, B., Helder, D., 2009: Summary of current radiometric calibration coefficients for Landsat MSS, TM, ETM+, and EO-1 ALI sensors. *Remote Sensing of the Environment*, 113 (5), 893–903. doi.org/10.1016/j.rse.2009.01.007.

Crawford, C., Roy, D., Arab, S., Barnes, C., Vermote, E., Hulley, G., Gerace, A., Choate, M., Engebretson, C., Micijevic, E., Schmidt, G., Anderson, C., Anderson, M., Bouchard, M., Cook, B., Dittmeier, R., Howard, D., Jenkerson, C., Kim, M., Kleyians, T., Maiersperger, T., Mueller, C., Neigh, C., Owen, L., Page, B., Pahlevan, N., Rengarajan, R., Roger, J., Sayler, K., Scaramuzza, P., Skakun, S., Yan, L., Zhang, H., Zhu, Z., Zahn, S., 2023: The 50-year Landsat collection 2 archive. Science of Remote Sensing, 8, 100103. doi.org/10.1016/j.srs.2023.100103.

Ding, H. Elmore, A., 2015: Spatio-temporal patterns in water surface temperature from Landsat time series data in the

Chesapeake Bay, USA. *Remote Sensing of Environment*, 168, 335–348. doi:10.1016/j.rse.2015.07.009

Dyba, K., Ermida, S., Ptak, M., Piekarczyk, J., Sojka, M., 2022: Evaluation of methods for estimating lake surface water temperature using Landsat 8. *Remote Sensing*, 14(15), 3839. doi.org/10.3390/rs14153839.

Fuso, F., Stucchi, L., Bonacina, L., Fornaroli, R., Bocchiola, D., 2023: Evaluation of water temperature under changing climate and its effect on river habitat in a regulated Alpine catchment. *Journal of Hydrology*, 616, 128816. doi.org/10.1016/j.jhydrol.2022.128816.

Gerace, A., Kleynhans, T., Eon, R., Montanaro, M., 2020: Towards an operational, split window-derived surface temperature product for the thermal infrared sensors onboard Landsat 8 and 9. *Remote Sensing*, 12(2), 224. doi.org/10.3390/rs12020224.

GCOS, 2016: The global observing system for climate: Implementation needs. *World Meteorological Organization*, 200, 316.

Irons, J., Dwyer, J., Barsi, J., 2012: The next Landsat satellite: The Landsat data continuity mission. *Remote sensing of environment*, 122, 11-21. doi.org/10.1016/j.rse.2011.08.026.

Jiménez-Muñoz, J., Sobrino, J., Skoković, D., Mattar, C., Cristóbal, J., 2014: Land surface temperature retrieval methods from Landsat-8 thermal infrared sensor data. *IEEE Geoscience Remote Sensing Letters*, 11(10), 1840–1843. doi.org/10.1109/LGRS.2014.2312032.

Jungkeit-Milla, K., Pérez-Cabello, F., de Vera-García, A., Galofré, M., Valero-Garcés, B., 2024: Lake Surface Water Temperature in high altitude lakes in the Pyrenees: Combining satellite with monitoring data to assess recent trends. *Science of the Total Environment*, 933, 173181. doi.org/10.1016/j.scitotenv.2024.173181.

Malakar, N., Hulley, G., Hook, S., Laraby, K., Cook, M., Schott, J., 2018: An Operational Land Surface Temperature Product for Landsat Thermal Data: Methodology and Validation. *IEEE Transactions on Geoscience and Remote Sensing*, 56(10), 5717-5735. doi.org/10.1109/TGRS.2018.2824828.

Markham, B., Storey, J., Williams, D., Irons, J., 2004: Landsat sensor performance: history and current status. *IEEE transactions on geoscience and remote sensing*, 42(12), 2691-2694. doi.org/10.1109/TGRS.2004.840720.

Meng, X., Cheng, J., Zhao, S., Liu, S., Yao, Y., 2019: Estimating land surface temperature from Landsat-8 data using the NOAA JPSS enterprise algorithm. *Remote Sensing*, 11(2), 155. doi.org/10.3390/rs11020155.

NASA, 2024: Available on Web: https://landsat.gsfc.nasa.gov/data/handbooks-guides/.

Niclòs, R., Perelló, M., Puchades, J., Coll, C., Valor, E., 2023: Evaluating Landsat-9 TIRS-2 calibrations and land surface temperature retrievals against ground measurements using multi-instrument spatial and temporal sampling along transects. *International Journal of Applied Earth Observation and Geoinformation*, 125, 103576. doi.org/10.1016/j.jag.2023.103576.

Olmanson, L., Brezonik, P., Finlay, J., Bauer, M., 2016: Comparison of Landsat 8 and Landsat 7 for regional measurements of CDOM and water clarity in lakes. Remote Sensing of the Environment, 185, 119–128. doi.org/10.1016/j.rse.2016.01.007

Singh, M., Saha, R., Saha, H., Sahoo, A., Biswal, A., 2018: Effects of sub-lethal doses of miconazole nitrate on *Labeo rohita* and its curing efficacy against Saprolegniasis. Aquaculture, 495, 205–213. doi.org/10.1016/j.aquaculture.2018.04.029.

Tavares, M., Cunha, A., Motta-Marques, D., Ruhoff, A., Cavalcanti, J., Fragoso C., Bravo, J., Munar, A., Fan, F., Rodrigues, R., 2019: Comparison of methods to estimate lake-surface-water temperature using Landsat 7 ETM+ and MODIS imagery: Case study of a large shallow subtropical lake in southern Brazil. Water, 11(1), 168. doi.org/10.3390/w11010168.

Vanhellemont, Q., 2020: Automated water surface temperature retrieval from Landsat 8/TIRS. *Remote Sensing of Environment*, 237, 111518. doi.org/10.1016/j.rse.2019.111518.

Wulder, M., Roy, D., Radeloff, V., Loveland, T., Anderson, M., Johnson, D., Healey, S. Zhu, Z., Scambos, T., Pahlevan, N., Hansen, M., Gorelick, N., Crawford, C., Masek, J., Hermosilla, T., White, J., Belward, A., Schaaf, C., Woodcock, C., Huntington, J., Cook, B. 2022: Fifty years of Landsat science and impacts. *Remote Sensing of Environment*, 280, 113195. doi.org/10.1016/j.rse.2022.113195.

Yu, X., Guo, X., Wu, Z., 2014: Land surface temperature retrieval from Landsat 8 TIRS - Comparison between radiative transfer equation-based method, split window algorithm and single channel method. *Remote sensing*, 6(10), 9829-9852. doi.org/10.3390/rs6109829.